NANO · MICRO small
www.small-journal.com

Hybrid Nanofibrous Composites with Anisotropic Mechanics and Architecture for Tendon/Ligament Repair and Regeneration

Jun Li, Chao Xue, Hao Wang, Shiyan Dong, Zhaogang Yang, Yuting Cao, Binan Zhao, Biao Cheng, Xianrui Xie, Xiumei Mo, Wen Jiang, Hengfeng Yuan,* and Jianfeng Pan**

Rupture of tendons and ligaments (T/L) is a major clinical challenge due to T/L possess anisotropic mechanical properties and hierarchical structures. Here, to imitate these characteristics, an approach is presented by fabricating hybrid nanofibrous composites. First, hybrid fiber-reinforced yarns are fabricated via successively electrospinning poly(L-lactide-co-ε-caprolactone) (PLCL) and gelatin (Ge) nanofibers onto polyethylene terephthalate (PET) fibers to improve biodurability and biocompatibility. Then, by comparing different manufacturing methods, the knitted structure succeeds in simulating anisotropic mechanical properties, even being stronger than natural ligaments, and possessing comfort compliance superior to clinically used ligament advanced reinforcement system (LARS) ligament. Moreover, after inoculation with tendon-derived stem cells and transplantation in vivo, hybrid nanofibrous composites are integrated with native tendons to guide surrounding tissue ingrowth due to the highly interconnected and porous structure. The knitted hybrid nanofibrous composites are also ligamentized and remodeled in vivo to promote tendon regeneration. Specifically, after the use of optimized anisotropic hybrid nanofibrous composites to repair tendon, the deposition of tendon-associated extracellular matrix proteins is more significant. Thus, this study indicates a strategy of manufacturing anisotropic hybrid nanofibrous composites with superior mechanical properties and good histocompatibility for clinical reconstruction.

1. Introduction

Tendons and ligaments (T/L) take the form of cords or straps with oval cross-section. The forces developed from skeletal muscles are transferred to bones by connective tissue of tendons. The bones are bound together by the fibrous articulation of ligaments to allow varying degrees of movement.[1,2] As specialized supporting connective tissues, T/L contain fascicles of type I collagen that orientate primarily parallel to the long axis, but interwoven to some extent. In the loose framework between collagen fasciculi, smaller blood vessels ramify and give off capillary plexus to provide nutrients for collagen fascicles. It is not surprising to find that T/L are viscoelastic like other biological tissues, as well as being anisotropic and inhomogeneous.[3–5] Due to this unique structural feature, T/L are easier to split along its grain than against it in cross-section. The multiscale hierarchical structure of collagen fibers arranged in a longitudinally striated appearance give

J. Li, C. Xue, B. Zhao, B. Cheng, J. Pan
Department of Orthopedics
Shanghai Tenth People's Hospital
School of Medicine
Tongji University
Shanghai 200072, P. R. China
E-mail: jianfengpan@tongji.edu.cn

H. Wang
Department of Orthopedics
The Second Affiliated Hospital of Chongqing Medical University
Chongqing 400010, P. R. China

S. Dong, Z. Yang, W. Jiang
Department of Radiation Oncology
The University of Texas MD Anderson Cancer Center
Houston 77030, USA
E-mail: wjiang4@mdanderson.org

The ORCID identification number(s) for the author(s) of this article can be found under https://doi.org/10.1002/smll.202201147.

Y. Cao, H. Yuan
Department of Orthopaedics
Shanghai Sixth People's Hospital
Shanghai Jiaotong University
Shanghai 200233, P. R. China
E-mail: yuanhf@shsmu.edu.cn

X. Xie
School of Pharmacy
Key Laboratory of Prescription Effect and Clinical Evaluation of State Administration of Traditional Chinese Medicine of China
Binzhou Medical University
Yantai 264003, P. R. China

X. Mo
State Key Laboratory for Modification of Chemical Fibers and Polymer Materials
Donghua University
Shanghai 201620, P. R. China

DOI: 10.1002/smll.202201147

 © 2022 Wiley-VCH GmbH

them high mechanical strength. Duplicating such properties of excellent mechanical performance remains an unswerving pursuit to produce resilient and durable synthetic biomaterials. To mimic T/L, the anisotropic architecture should be achieved and controlled to satisfy both the mechanical strength profile and the biological properties, which remains highly challenging.[6,7]

At the microstructural level, T/L are composites arranged with multiple levels of hierarchy. Their properties are highly anisotropic, and the ideal strategy to mimic them is to adopt fiber-reinforced composites. Medical fibrous artificial ligament is one of the most popular and representative scaffolds for T/L repair, owing to its conformability and functionality.[8] When fabricating appropriate medical biotextiles as T/L grafts, polymer selection, and fiber configuration design must be considered so that to match the specific requirements. Various staple fibers formulated from synthetic polymers, natural polymers, or biopolymers have been used to produce artificial ligaments over the past 40 years. Starting from the 1980s, various materials were evaluated and developed to serve as artificial ligaments, such as nylon, carbon (Intergraft), polytetrafluoroethylene (PTFE) (Gore-Tex), polyester (Dacron, Proflex, Trevira, Leeds-Keio ligament), polypropylene (Polyflex, Kennedy Ligament Augmentation Device).[9] Today, only polyethylene terephthalate (PET) is still used as T/L graft clinically since it is reasonably inert, flexible, resilient, durable, and resistant to biological degradation. PET has withstood the test of time, whereas other materials have not proven to be durable when used in an implant application.[10–12] Ligament advanced reinforcement system (LARS) ligament is a medical fabric composed of PET fibers for anterior cruciate ligament reconstruction. The both ends of LARS ligament are designed as woven structure for bony insertion, and the middle part is composed of nonwoven straight fibers as an intra-articular component.[13,14] Although LARS ligament has been reported with excellent mechanical strength to achieve promising short-term clinical outcomes, it is evident that only a set of straight fibers does not constitute a successful, functioning ligament graft in the long-term. 50% re-rupture rate and 63% osteoarthritis rate were presented along with foreign body synovitis, chronic effusion, and recurrent instability.[15,16] The principal causes for synthetic T/L graft excision and revision surgery were ruptures and synovitis.[17] According to these drawbacks, careful consideration of fiber configuration design is necessary when deciding on fiber structure to be incorporated into the construction of T/L grafts.

In determining the long-term success of synthetic grafts for T/L repair and regeneration, the textile structure has been proven to play a crucial role.[18,20] Through retrospective analysis of synthetic ligamentous grafts, there are three most common mechanisms for graft failure including: inadequate abrasion resistance between host insertion sites and synthetic grafts (yarn-on-tissue abrasion), poor fatigue properties due to loose fiber-to-fiber abrasion (yarn-on-yarn abrasion), and poorly organized, incomplete tissue growth inside the grafts.[21] All these mechanisms were associated with the configuration of structural design. In any model of synthetic grafts, the abrasion of textile fibers derived from yarn-on-yarn or yarn-on-tissue was a common phenomenon.[22] For LARS ligament, the intra-articular component is loose PET fibers. During flexural and torsional movements, fiber-to-fiber abrasion occurs to deteriorate the fatigue resistance, resulting in fiber axial splitting and graft failure. Thus, how to design the architecture to avoid fiber-to-fiber abrasion is pivotal to ensure the long-term functionality of PET grafts. Electrospinning technique can be used to reinforce PET fibers into tight nanofibrous yarns. Poly(L-lactide-co-ε-caprolactone) (PLCL), as a commonly used electrospinning material, is hydrophobic aliphatic polyester copolymers obtained by ring-opening polymerization of polylactic acid (PLA) and polycaprolactone (PCL) monomers at the mass ratio of 75:25. Due to its hydrophobicity, PLCL can prevent inner PET fibers from bioabrasion and biocorrosion.

In this work, a new type artificial ligament of anisotropic hybrid fiber-reinforced composites was fabricated via the combination of electrospinning technique and knit process. (**Scheme 1**) PET fibers were used as base materials for inner core. PLCL was electrospun as an intermediate sheath to bond PET fibers together to enhance durability. Then gelatin nanofibrous matrices were coated and subsequently crosslinked in the outer layer to obtain desired biocompatibility. Through this tricomponent fiber process technology, anisotropic hybrid nanofibrous yarns were produced from PET fibers, PLCL polymeric substrates, and gelatin nanofibrous matrices in the transverse order. The final fiber-reinforced composites were formed by knitting hybrid yarns in horizontal rows and vertical columns. At the microstructural level, the longitudinal orientation and transverse succession of PET fibers, PLCL, and gelatin nanofibrous matrices determined the anisotropic structural behavior of PET-PLCL-Ge composites. At the macrostructural level, continuous pores were formed in the 3D architecture to provide optimal spatial organization and nutritional conditions for tissue ingrowth, which also resulted in minimal contact between knitted yarns to avoid further abrasion. The major concern in engineering anisotropic fiber-reinforced composites was the spatial organization of the elements so as to obtain desired mechanical and biological properties. Our study provided a combination of fabrication technique, fiber process, and composite technology to construct controlled architectural structure for T/L repair and regeneration.

2. Results and Discussion

2.1. Fabrication and Structural Analysis of Anisotropic Hybrid Nanofibrous Yarns

Since T/L are characterized by anisotropic properties, fiber-reinforced composites are designed and synthesized to match their specific requirements. The final properties of fabricated composites were strongly affected by the properties, distribution, content of constituent materials, and the interaction among them.[23] To obtain superior mechanical strength we selected PET fibers as the base material. Due to the fineness of individual fibers, it was necessary to bring PET fibers together into a thicker bundle to mimic the tendinous bundle. Within the PET bundle, each of filaments was identical. The inner array of PET filaments was longitudinal and the number of fibers could be adjusted. The diameter varied with the number of fibers to adapt to different scenarios, especially when implanted in areas that required high mechanical strength or

© 2022 Wiley-VCH GmbH

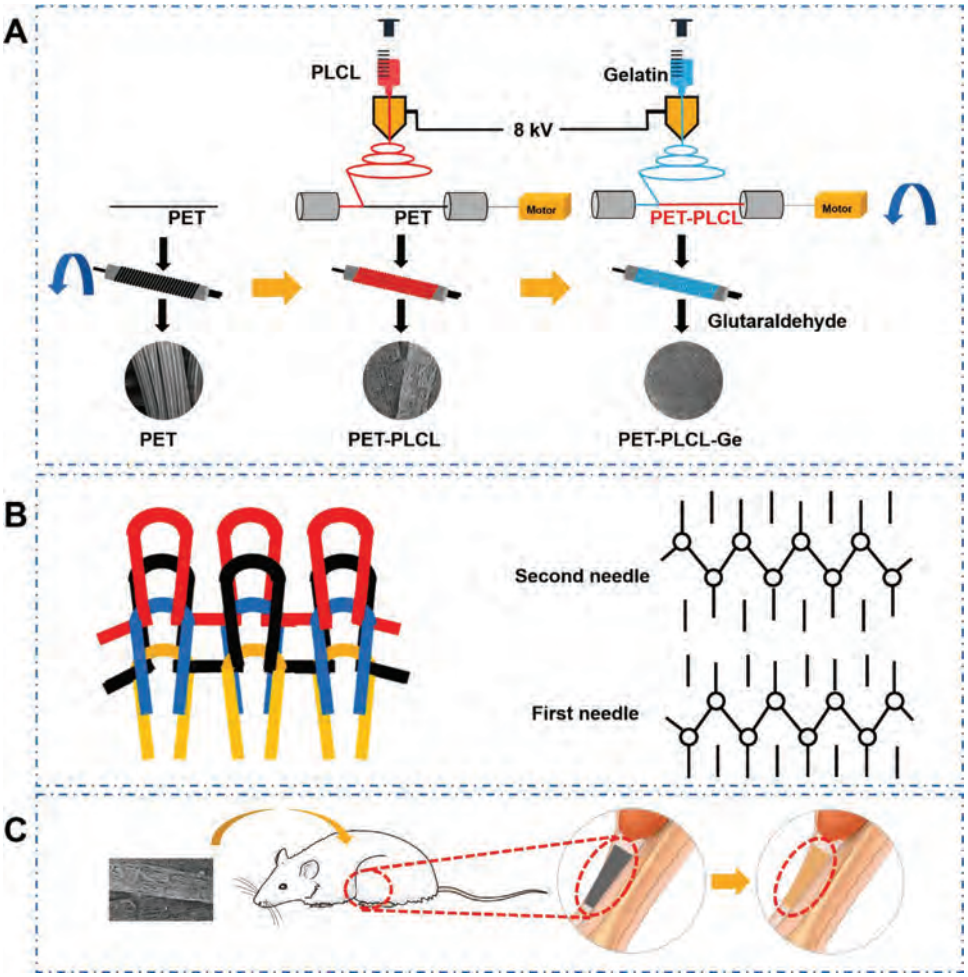

Scheme 1. A) Preparation of PET-PLCL-Ge tricomponent yarn. PET fibers were used as the inner core, PLCL and gelatin nanofibers were successively electrospun as an intermediate and outer sheath to bond PET fibers together and obtain better biocompatibility. B) Hybrid nanofibrous composites were fabricated through interloping PET-PLCL-Ge yarns in horizontal rows and vertical columns of stitches. C) Knitted nanofibrous composites with anisotropic mechanics and architecture were used to promote tendon/ligament repair and regeneration.

thickness. In this study, there were 48 filaments in the individual PET yarn (**Figure 1**A). The average diameter of PET fibers was 21.50 ± 1.64 um. The analysis of diameter distribution histogram showed that PET fibers had a relatively homogeneous morphology (Figure 1B).

From cross-section view of PET bundle, the individual fibers were arranged in a scattered and loose state, which was not conducive to durability and fatigue resistance (Figure 1A). To prevent fibers from axially splitting and dispersing, electrospinning technology was used to wrap PET fibers at microstructural level. PLCL nanofibrous matrices were manufactured as a sheath to limit fiber-to-fiber movement and increase durability. The electrospun PLCL nanofibers were preferentially oriented along axial direction to maintain anisotropic characteristics. It bound PET fibers together and avoided PET fibers sliding relative to each other so to prevent damage associated with fiber-to-fiber abrasion. After electrospinning axially aligned PLCL nanofibers as wrapping layer, PET fibers were gathered into a tight bundle (Figure 1A). From morphological view of PET-PLCL yarn, we found that PLCL nanofibers were smooth, continuous, and axially aligned. The average diameter of PLCL nanofibers was 779.91 ± 159.75 nm. The histogram of diameter distribution showed that PLCL nanofibers were uniform in diameter (Figure 1B).

As with all biological scaffolds implanted in vivo, the question of biocompatibility is paramount for hybrid composites.[24,25] They were composed of two or more materials, the probability of causing adverse tissue reactions was greatly enhanced. After implantation, adverse reactions primarily occurred in the interface between scaffolds and host tissue matrix.[26] In our study, after wrapping PET fibers with PLCL nanofibers, gelatin nanofibers were subsequently electrospun in axially aligned orientation to create a biocompatible interface. Unlike conventional composites in which tissue or blood were exposed to multiple polymers simultaneously, in this PET-PLCL-Ge tricomponent yarn, only gelatin sheath made initial contact with host tissue in vivo. As shown in Figure 1C, PET showed the largest water contact angle and exhibited obvious hydrophobicity that unfavorable for cell growth. After PLCL was wrapped, it still showed hydrophobicity. But after gelatin was wrapped, the water contact angle was significantly reduced and hydrophilicity was achieved to support cell growth. From morphological

 © 2022 Wiley-VCH GmbH

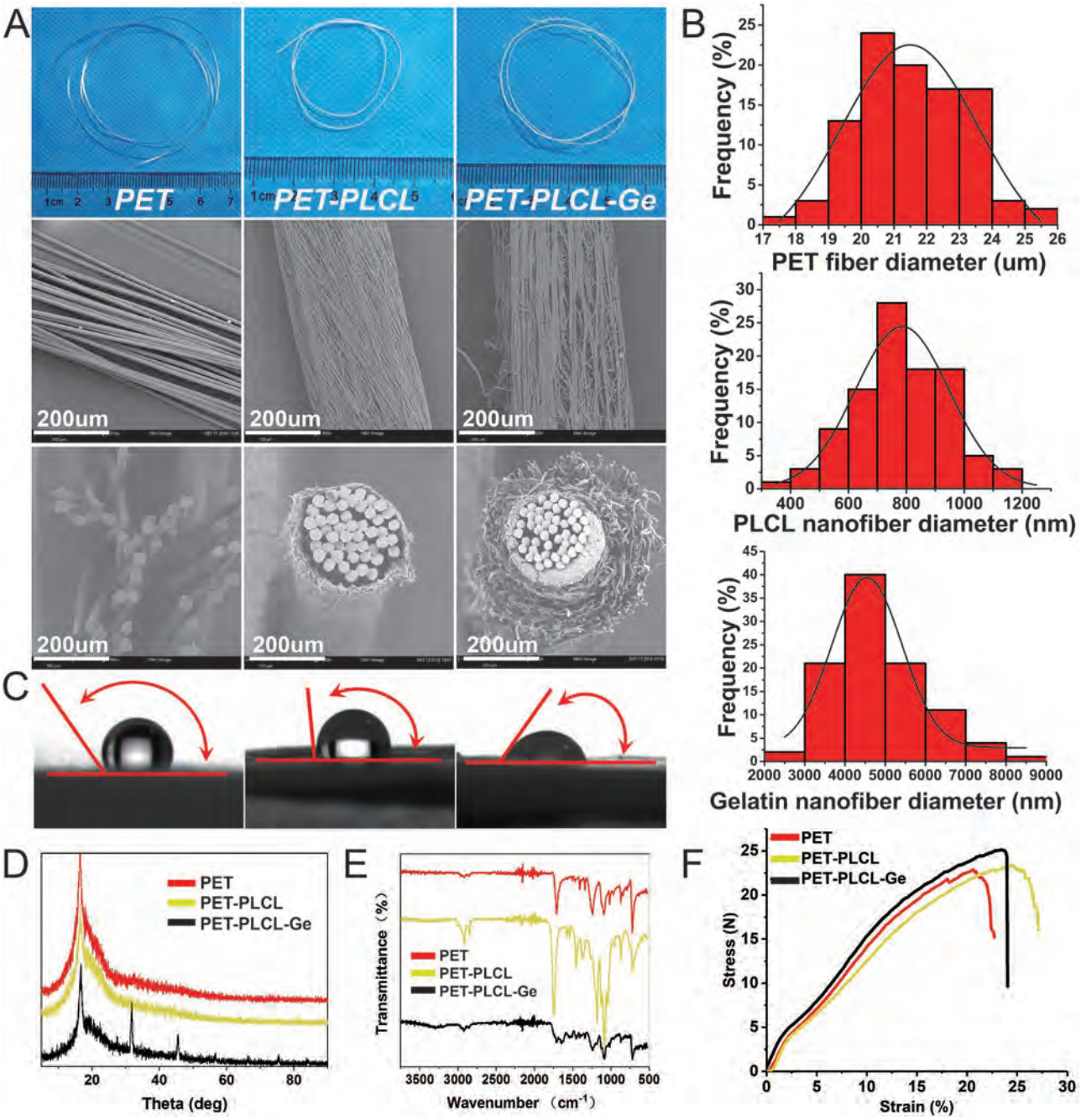

Figure 1. A) General views and SEM images of hybrid PET, PET-PLCL, and PET-PLCL-Ge yarns. B) The diameter distribution histogram of inner PET fibers, intermediate PLCL nanofibers and outer gelatin nanofibers. (n = 100) C) Water contact angles of PET, PET-PLCL, and PET-PLCL-Ge yarns. D,E) XRD and FTIR spectra of PET, PET-PLCL, and PET-PLCL-Ge yarns. F) Comparison of stress-strain curves for PET, PET-PLCL, PET-PLCL-Ge yarns.

view of PET-PLCL-Ge yarn, gelatin nanofibers were mostly arranged in axial direction. The fiber diameter ranged primarily from 3.0 to 6.0 um, with an average diameter of 4.86 um, which was higher than PLCL nanofibers (Figure 1B).

Then, XRD and FTIR spectra were conducted to confirm the successful electrospinning wrap of PLCL and gelatin nanofibers (Figure 1D,E). The crystallization was determined through the position and intensity of diffraction peaks in XRD spectra. For PET yarn, a crystalline diffraction peak appeared at about 17.1°. After electrospinning PLCL nanofibers, there was no new crystalline diffraction peak, indicating that the electrospinning of PLCL had no particular effect on crystallization. For PET-PLCL-Ge yarn, new crystalline diffraction peaks appeared at 32.1° and 45.9°, demonstrating that the crystallization was increased as a consequence of electrospinning and crosslinking of gelatin nanofibers. In FTIR spectra, a characteristic band of PET was centered at 1715, 1245, 1100, and 730 cm^{-1}, which were assigned to ketones (C=O), ether aromatic (C–O), ether

 © 2022 Wiley-VCH GmbH

aliphatic (C–O) and aromatic (C-H) bond. Compared with PET, PET-PLCL yarn showed the same peaks mentioned above and new peak at 1755 cm^{-1} was corresponding to PLCL. PET-PLCL-Gel yarn exhibited the characteristic protein bands at 1651^{-1} cm for amide I (C=O stretching) and 1549^{-1} cm for amide II (N–H bending vibration), respectively.

Next, we compared the mechanical properties of PET, PET-PLCL, and PET-PLCL-Ge yarns. PET fibers were aligned in the long axis direction to maintain mechanical strength. Compared with PET, PET-PLCL and PET-PLCL-Ge yarns showed no significant increase in tensile strength (Figure 1F). This was mainly due to the fact that PET filaments in core were several orders thicker than nanofibers in wrapping layers. So, PET fibers played the dominant role in final mechanical strength. Around the inner PET filaments, the constituents of PLCL and gelatin nanofibers were arranged transversely in succession. The sheath of PLCL limited fiber-to-fiber abrasion to improve fatigue resistance. Considering the biostability of PET and PLCL, as well as the bioabsorbability of gelatin, we selected PET-PLCL as inner core. As a consequence, the structure of PET-PLCL-Ge yarn did not change dramatically even if the outer gelatin matrices were dissolved after implantation for a certain period. This distribution characteristic is beneficial to enhance the durability of hybrid nanofibrous yarns.

Therefore, by using this tricomponent fiber processing technology, it is available to engineer mechanical strength and improve biological properties at the same time to meet medical requirements of ligament graft application. If necessary, therapeutic agents can also be incorporated into gelatin matrices and delivered at modulated rates depending on the thickness of electrospun layer. The arrays of hybrid tricomponent yarn were anisotropic that they contained both longitudinally aligned nanofibers and transversally laminated substrates. Through wrapping different sheaths we engineered mechanical properties independently in the axial and cross directions.

2.2. Textile Configuration Analysis of Anisotropic Fiber-reinforced Composites

Based on aforementioned three laminate structure, an anisotropic hybrid nanofibrous yarn was produced. After that, it was fabricated into 3D hierarchical structure to obtain the desired mechanical and biological properties. Typical textile configurations applied in medical applications include nonwovens, wovens, and knits. Nonwoven is fabricated directly from nanofibers without the intermediate process of producing yarn. The nanofibers can be oriented randomly or primarily aligned in one direction.[27] In this study, nonwoven fabrics were produced by using electrospinning technique so as to compare with other textile configurations. PET, PET-PLCL, and PET-PLCL-Ge nonwoven substrates were formed by electrospinning PET, PLCL, and gelatin nanofibers sequentially onto the grounded rotating collector (**Figure 2**A). By the application of a high voltage electrostatic field (5–30 kV), PET, PLCL, and gelatin nanofibers overcame the surface tension, bonded and interlocked together by means of mechanical and thermal action. From gross morphology, the nonwoven substrate exhibited a two-dimensional structure that resembled paper in appearance (Figure 2A). Observed under scanning electron microscope, all nonwoven fabrics presented interconnected webs of fine nanofibers (Figure 2A). The average pore size of nonwoven fabrics was under a single distribution that was associated with the diameter and density of nanofibers. Compared with PET and PET-PLCL nonwoven substrates, PET-PLCL-Ge exhibited a smaller water contact angle and better hydrophilic properties after electrospinning of gelatin nanofibers. This was consistent with the hydrophilicity result of the hybrid nanofibrous yarn after electrospinning the third gelatin layer on the surface of nano yarn.

Different from nonwoven electrospinning substrates, woven and knitted structures involve the interweaving of a series of yarns, resulting in a three-dimensional controlled regular structure. Compared with two-dimensional structure, the three-dimensional structure of scaffolds simulates natural microenvironment, providing space for tissue ingrowth and allowing diffusion of nutrient to the cells.[28,29] Various structural forms can be achieved by using the three-dimensional braiding technique. In this study, the woven was produced from the primary structural yarns that were oriented in warp and weft direction. Due to the orthogonal relationship of warp and weft yarns, the woven fabric presented an interwoven dense structure with yarns oriented at 90° to each other (Figure 2B). As illustrated from SEM observation, there was no obvious pore structure in the PET woven fabrics. We compared it with the LARS ligament that also used woven braiding technique and found that both of them showed low porosities in appearance (Figure 2C). This will result in low water/blood permeability, which is unfavorable for surrounding tissue ingrowth.

Subsequently, we analyzed the structural characteristics of knitted fabrics. Unlike woven structure, knitted construction was fabricated through interloping yarns in horizontal rows and vertical columns of stitches. As a result, a porous structure with interconnected pores was produced from interloping yarns (Figure 2D). Compared to isolated pore structure, an interconnected pore network can enhance the diffusion rates to and from the center of the scaffold and facilitate vascularization, thus improving oxygen and nutrient supply and waste removal. Moreover, the porous structure induced the knitted fabrics to be softer, more flexible, and easily conformable. As shown in Figure 2E, LARS ligament and woven fabrics showed rigid stiffness and were not easily flexible in warp and weft directions due to low porosity and orthogonal dense structure. Although high breaking strength is achieved in woven structure, stiffer and less flexible properties make it more difficult to handle and suture. By contrast, the better handling characteristics make knitted fabrics more suitable for ligament graft application. During surgical procedure, the thickness of synthetic grafts ultimately used for T/L repair and regeneration can be controlled by sewing them together depending on the size and strength of the associated tendon/ligament.

Therefore, we prepared anisotropic fiber-reinforced composites from hybrid nanofibrous yarns through knitting technique. The primary structure of fiber-reinforced composites is the transverse sequence of nanofibrous substrates in the hybrid nanofibrous yarn: PET fibers for inner core, PLCL nanofibers for intermediate sheath, and gelatin nanofibrous matrices for outer layer. The secondary structure is the three-dimensional

 © 2022 Wiley-VCH GmbH

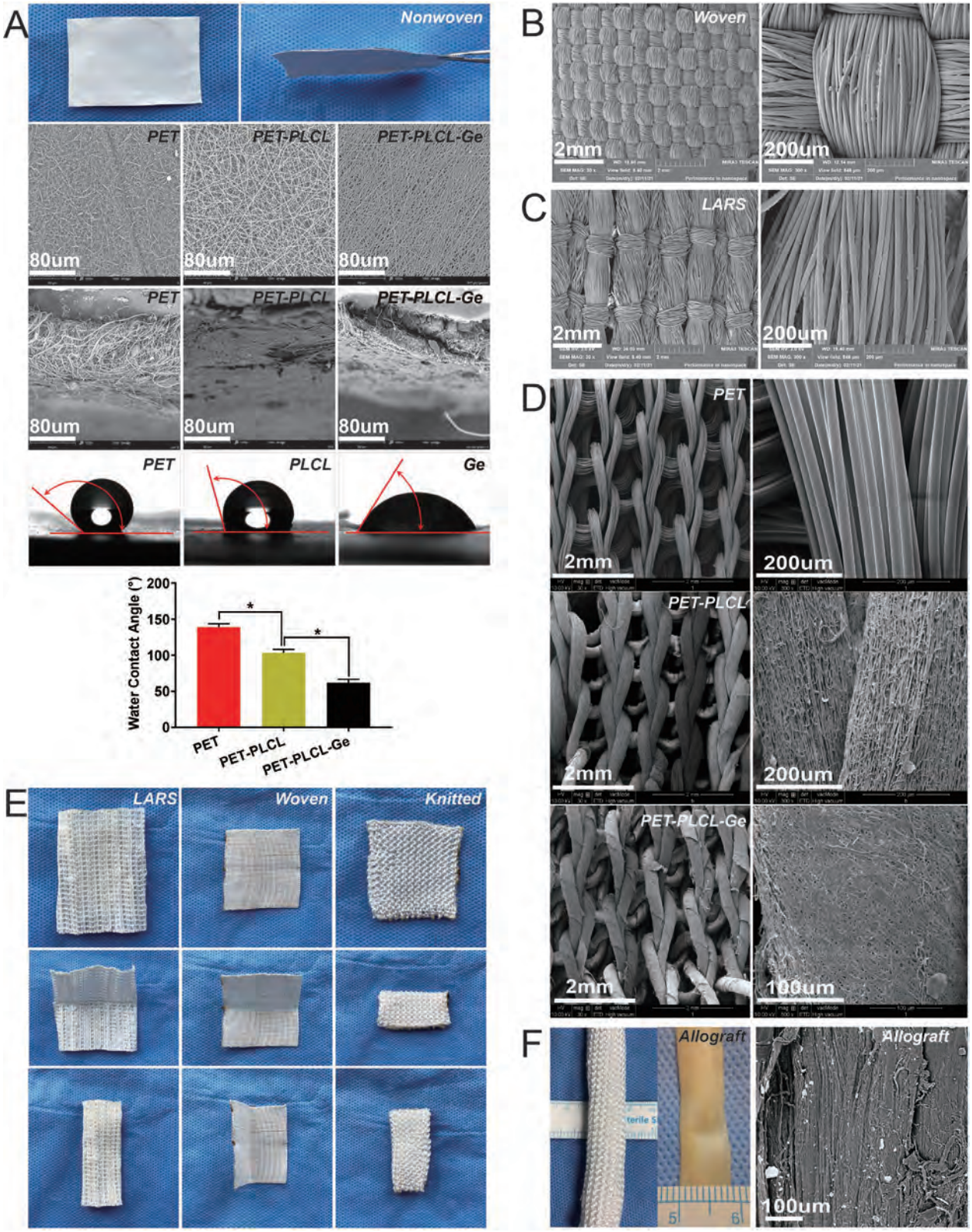

Figure 2. A) General views, SEM images, and water contact angles of nonwoven PET, PET-PLCL, and PET-PLCL-Ge scaffolds manufactured by electrospinning technique. Water contact angles were statistically analyzed by the Student's *t*-test. ($n = 3$; * represented $p < 0.05$.) B) SEM images of woven PET composite. C) SEM images of LARS ligament that were used in clinic. D) SEM images of knitted PET, PET-PLCL, and PET-PLCL-Ge composites. E) Compliance assessment of LARS, woven and knitted composites in warp and weft direction. F) Comparison of the artificial ligament from knitted PET-PLCL-Ge yarns with natural ligament (allograft) and SEM image of the natural ligament.

 © 2022 Wiley-VCH GmbH

architecture by interloping yarns to get an interconnected pore network. The pores between PET-PLCL-Ge yarns provide delicate space for the ingrowth of connective tissue, which surrounds artificial ligament fibers and forms their immediate external environment. It is the site of metabolic exchange between ligament fibers and blood, which contains capillary plexus and bundles of small nerve fibers. This more open structure was designed intentionally so as to make the graft easier to increase the extent of tissue incorporation into the grafts. The tertiary structure is overall three-dimensional structure of fiber-reinforced composites after roll up to a certain thickness. The tertiary structure is primarily due to the difference in the size and strength of the associated tendon/ligament that need repair or replacement. As with the two-level anisotropic structure and overall controlled thickness, various properties were also engineered into the composites to meet design goals including added flexibility, increased strength, controlled thickness, improved handling, and better suture holding strength. Finally, the anisotropic fiber-reinforced composites reached the equal thickness to natural T/L tissue while the microstructural appearance was identical to natural T/L tissue on the surface (Figure 2F).

2.3. Mechanical Properties of Anisotropic Hybrid Nanofibrous Composites

The ideal synthetic grafts for T/L repair and regeneration must simultaneously meet the following mechanical characteristic requirements.[30] 1) The axial tensile strength is equal to or exceeds the strength of natural T/L tissues. 2) The synthetic grafts must resist long-term creep deformation. 3) After high amount of cyclic loading, there is still no fatigue fracture and deformation for the synthetic grafts. 4) Abrasion of synthetic grafts should be reduced including fiber-to-fiber and fiber-to-tissue abrasion.

In natural T/L tissues, parallel collagen fibrils are arranged in bundles longitudinally with a wavy pattern, known as crimp. This structure plays a vital role in the nonlinear mechanical properties of T/L tissues to provide elasticity and prevent injury. As shown in **Figure 3**A, there was a toe-like (low stiffness) region followed by a linear elastic (higher stiffness) region for native tendon. Compared with it, knitted composites exhibited a smaller toe region and narrowed transition strain. This was due to the knitted structure of interloping yarns. For LARS ligament and woven composites, there were only alignment of PET fibers in the axial direction according to their SEM observation. Consequently, the stress-strain profile did not include the toe-like region followed by a linear elastic region. Therefore, knitted composites were partially successful in reproducing the nonlinear mechanical functionality of native T/L by knitting instead of crimped structure.

Then we compared the mechanical properties of native tendon, LARS, woven, and knitted ligaments (Figure 3B). At the breaking of axial stretch, LARS, woven, and knitted ligaments exhibited higher tensile strength than native tendon. The breaking elongation of LARS and woven ligaments was obviously inferior to that of native tendon. Due to the gradual unfolding of interloping yarns with increasing strain, the breaking elongation of knitted ligament was significantly higher than that of LARS and woven ligaments. Therefore, knitted ligament achieved satisfactory breaking elongation parallel to native tendon. In analyzing the anisotropy of mechanical properties, we found that both LARS and PET-PLCL-Ge knitted ligaments showed different tensile strengths in axial and lateral directions (Figure 3B). This feature was identical to native tendon, in which tensile strength in axial direction was obviously superior to that in the lateral direction. Unlike them, the tensile strength of woven ligament was substantially equal at axial and lateral direction (Figure 3B). Thus, PET-PLCL-Ge knitted ligament was successfully designed to mimic the anisotropic characteristic of mechanical properties in native tendon. The hybrid nanofibrous composites and native tendon were stronger and stiffer in the longitudinal direction than in the transverse direction.

Next, we assessed the mechanical durability of woven and knitted ligaments. After twenty times of cyclic loading-unloading, there were no significant changes in the tensile strength (Figure 3C). Compared with woven composite, knitted ligament exhibited a hysteresis loop. Typically, the hysteresis loop in the loading-unloading curves represented the energy dissipation of each cycle. This was also due to the knitted structure of interloping yarns. Then, abrasion assessment was performed by SEM microscopic observation after cycles of loading-unloading tests. As shown in Figure 3D, there was no detectable signs of tearing and peeling on the surface of individual fibers for the composites before and after cyclic loading-unloading movements. The presence of surface peeling was also not detected in LARS ligament (Supporting Information Figure S5), indicating that PET fibers were abrasion-resistant materials. As well as, the knitted ligament resisted long-term creep deformation (Figure 3E). No fatigue fracture or deformation was detected, which ensure the durability of anisotropic hybrid nanofibrous composites in mechanical properties.

Finally, we evaluated the knitted ligaments of three different compositions and compared them with natural ligament tissues in mechanical behavior. In the stress-strain curves, there were no significant differences among PET, PET-PLCL, and PET-PLCL-Ge knitted ligaments (Figure 3F). At the axial direction, PET-PLCL-Ge knitted ligament exhibited stronger tensile strength than native tendon, while showed no difference in breaking elongation (Figure 3G). This indicates that PET-PLCL-Ge knitted ligament can exert strong mechanical properties and will not deform and elongate after clinical use. In the lateral direction, the breaking elongation of PET-PLCL-Ge knitted ligament was superior to that of the natural ligament. This provides another advantage over natural ligament in that the superior lateral extension of knitted ligament can provide better compliance during torsional movements of knees, especially mimicking the torsional characteristics of anterior or posterior cruciate ligaments that derived from their two-bundle structure.

2.4. Cytotoxicity Measurement of Anisotropic Knitted Nanofibrous Composites In Vitro

Complications of LARS ligament have already been reported for many years, especially for synovitis. Glezos reported a

 © 2022 Wiley-VCH GmbH

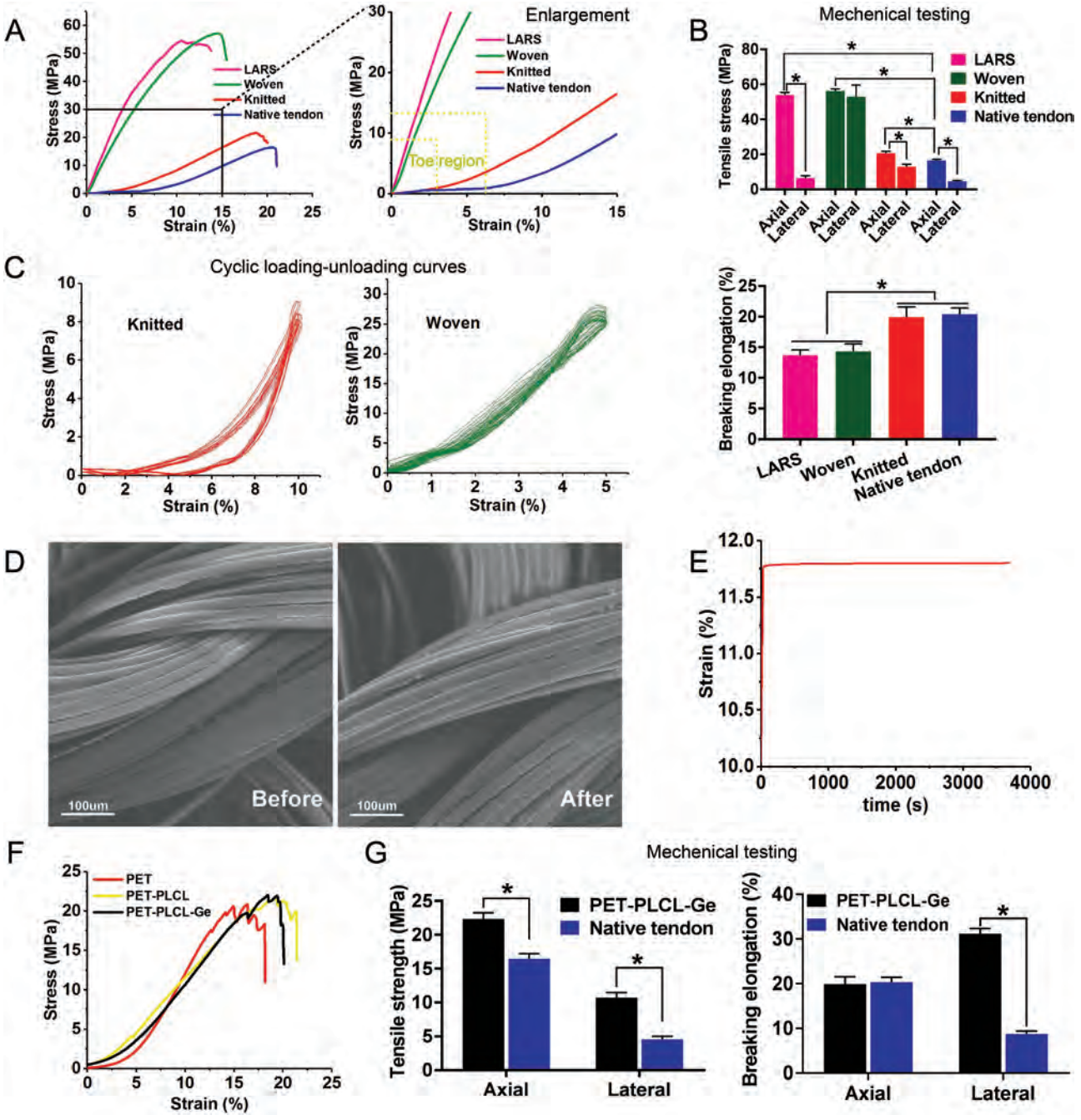

Figure 3. Mechanical testing of native tendon, LARS, woven and knitted ligaments. A) Stress-strain curves of native tendon, LARS, woven and knitted ligaments. B) Comparison of mechanical properties for native tendon, LARS, woven, and knitted ligaments. The data were statistically analyzed by the Student's *t*-test. ($n = 3$; * represented $p < 0.05$.) C) Cyclic loading-unloading curves of woven and knitted ligaments. ($n = 20$) D) Abrasion assessment of knitted and LARS ligaments was performed by SEM microscopic observation before and after cycles of loading-unloading tests. (LARS ligament was shown in Supporting Information Figure S5.) E) Long-term creep deformation for the knitted ligament. F) Stress-strain curves of knitted ligaments with three different compositions. G) Comparison of mechanical properties for PET-PLCL-Ge knitted ligament and native tendon. The data were statistically analyzed by the Student's *t*-test. ($n = 3$; * represented $p < 0.05$.)

rare case of disabling synovitis associated with LARS artificial ligament.[31] PET, as the component material for LARS ligament, was demonstrated to be hydrophobic by water contact angle assay in our study. Because of this unfavorable property, gelatin was electrospun outside as nanofibrous matrices to make the surface hydrophilic and more biocompatible. Prior to substituting native T/L, we paid attention to the biocompatibility measurement of knitted nanofibrous composites. Generally, cytotoxicity testing is the first step to screen biological scaffolds used for medical applications. In this study, knitted nanofibrous composites were initially tested for cytotoxicity in vitro and then their potential adverse

 © 2022 Wiley-VCH GmbH

effects on the host were evaluated through biocompatibility assays in vivo.

Under normal circumstances, native tendon has a very low metabolic rate. After the injury, its metabolism will increase markedly. Tendon-derived stem cells (TDSCs) are derived from tendon tissue and are significantly activated after injury to promote tendon regeneration and repair.[32,33] In this study, TDSCs were cultured to assess toxic effects of hybrid nanofibrous composites at cellular level. As illustrated in Supporting Information Figure S7, TDSCs were isolated from tendon tissue and exhibited universal stem cell characteristics, including clonogenicity, self-renewal, and multi-lineage differentiation capacities. TDSCs showed excellent proliferative capacity in vitro. After culturing in an adipogenic induction medium, multiple lipid droplets were formed and stained with oil red O, indicating that TDSCs differentiated into adipocytes. After osteogenic differentiation, multiple calcium deposits were detected and stained by alizarin red, revealing that TDSCs differentiated into osteocytes. In the induction of chondrogenic differentiation, TDSCs differentiated into chondrocytes, which was proven by alcian staining.

In the characterization of cultured TDSCs, flow cytometric analysis showed that 99.6% and 99.8% of TDSCs were positive for the specific markers of mesenchymal stem cell CD44 and CD90. Only 1.94% of TDSCs were positive for hematopoietic stem cell marker CD34 and 0.01% for endothelial cell marker CD31. This revealed that the isolated TDSCs possessed mesenchymal stem cell characteristics, but no hematopoietic stem cell or endothelial cell features (**Figure** 4A). The immunofluorescent staining also verified the positive of CD90 in TDSCs. Due to originating from tendon tissues, TDSC positively expressed tenocyte specific markers a-SMA and collagen I (Supporting Information Figure S7).

Then TDSCs were cultured on hybrid nanofibrous composites in vitro and the scaffolds friendly supported cell survival and proliferation. The number of viable cells in all groups increased with culture time (Figure 4B). Compared with PET and PET-PLCL composites, TDSCs in PET-PLCL-Ge composite showed a higher proliferative capacity after 10 days of cocultivation. This was associated with the hydrophilic gelatin nanofibers in outer layer to promote biocompatibility. When evaluating cell attachment on the knitted yarns, we also found that the number of TDSCs in PET-PLCL-Ge yarn was significantly higher than that in PET and PET-PLCL yarns (Figure 4C). Poor attachment property presenting in PET and PET-PLCL yarns was due to the hydrophobicity of PET and PLCL nanofibers. Gelatin nanofibers were favorable for cell attachment due to their hydrophilicity. Moreover, after DAPI and Phalloidin staining of TDSCs, we found that superior cell spreading was exhibited in PET-PLCL-Ge yarn (Figure 4 D,E). Compared with PET and PET-PLCL yarns, TDSCs in PET-PLCL-Ge yarn extended the cytoplasm for a larger adhesive area. The cell spreading area was statistically greater in PET-PLCL-Ge yarn than PET and PET-PLCL yarns (Figure 4D). The larger spreading area of PET-PLCL than PET was derived from the structure of nanofibrous matrices in PLCL layer. When the structure of nanofibrous matrices and the inherent property of gelatin to promote adhesion acted in a synergistic way, PET-PLCL-Ge yarn exerted the best performance on cell attachment and spreading (Figure 4E). The spreading area in PET yarn ranged primarily from 300 to 800 um^2. After electrospinning of PLCL nanofibers, the cell area increased to the range of 400–1200 um^2. In the PET-PLCL-Ge yarn, the cell spreading area is almost all larger than 1000 um^2 (Figure 4F).

2.5. Biocompatibility and Biodurability of Anisotropic Knitted Nanofibrous Composites In Vivo

Besides the cytotoxic effects of hybrid nanofibrous composites at the cellular level, we also paid attention to the biocompatibility of scaffolds with surrounding tissues, as well as the long-lasting secure functioning of composite grafts implanted in the recipients. Biocompatibility was the minimal adverse effect of biological scaffolds on the host. In this study, we evaluated the biocompatibility in vivo through systemic toxicity and local tissue reaction assays (**Figure 5**). Systemic toxicity was based on interference with key physiological functions and depended on the duration of exposure. Unfavorable scaffold-host interactions persisted to affect the physiological functions of vital organs and accumulated to endanger continued life. After 8 weeks of subcutaneous implantation, all rats survived healthily and no death was observed, indicating that constituents of nanofibrous composites were not potentially toxic and fatal. The microscopic structure of vital organs was also histologically analyzed to evaluate the systemic effects of nanofibrous composites on the host. If the scaffolds exhibit potential toxicity to the homeostatic environment in vivo, inflammatory cells and related mediators may be produced to affect the function and structure of visceral organs at other sites. The results showed that all organs were normal including heart, liver, spleen, kidney, and lungs. Whether after 4 weeks or 8 weeks, there was no inflammatory cell infiltration and tissue necrosis observed in visceral organs (Figure 5A). Moreover, local tissue reaction assays showed that the tissues surrounding nanofibrous composites had no obvious foreign body rejection, inflammation, tissue swollen, exudation, necrosis, etc. (Figure 5B,C) Therefore, whether systemic toxicity or local scaffold-host interactions, all tests demonstrated that anisotropic hybrid nanofibrous composites presented no harm to the host. The confirmation of safety and biocompatibility guaranteed nanofibrous composites towards T/L repair in vivo and ultimate human clinical use.

The long-term functionality depended on the biodurability of nanofibrous composites in vivo. Biodurability in medical applications was the situation that the host exerted minimal adverse effects of biodegradation and biocorrosion on the constituent materials. The durability of PET was associated with its non-degradation and thermal stability. After implantation for 8 weeks, there was no biological degradation observed for PET fibers (Figure 5C). PET's inherent properties, such as hydrophobicity, chemical inertness, and biodegradation resistance provide a theoretical basis for its biodurable property.

However, material selection cannot be governed solely by considerations of stability, and mechanical and physical properties especially may be of considerable importance. Biocorrosion was a surface phenomenon, in which the surface contact with body fluids adsorbed proteinaceous components, cellular elements, soluble components of water and ions, and subsequently initiated chemical corrosion. Between the contact area

 © 2022 Wiley-VCH GmbH

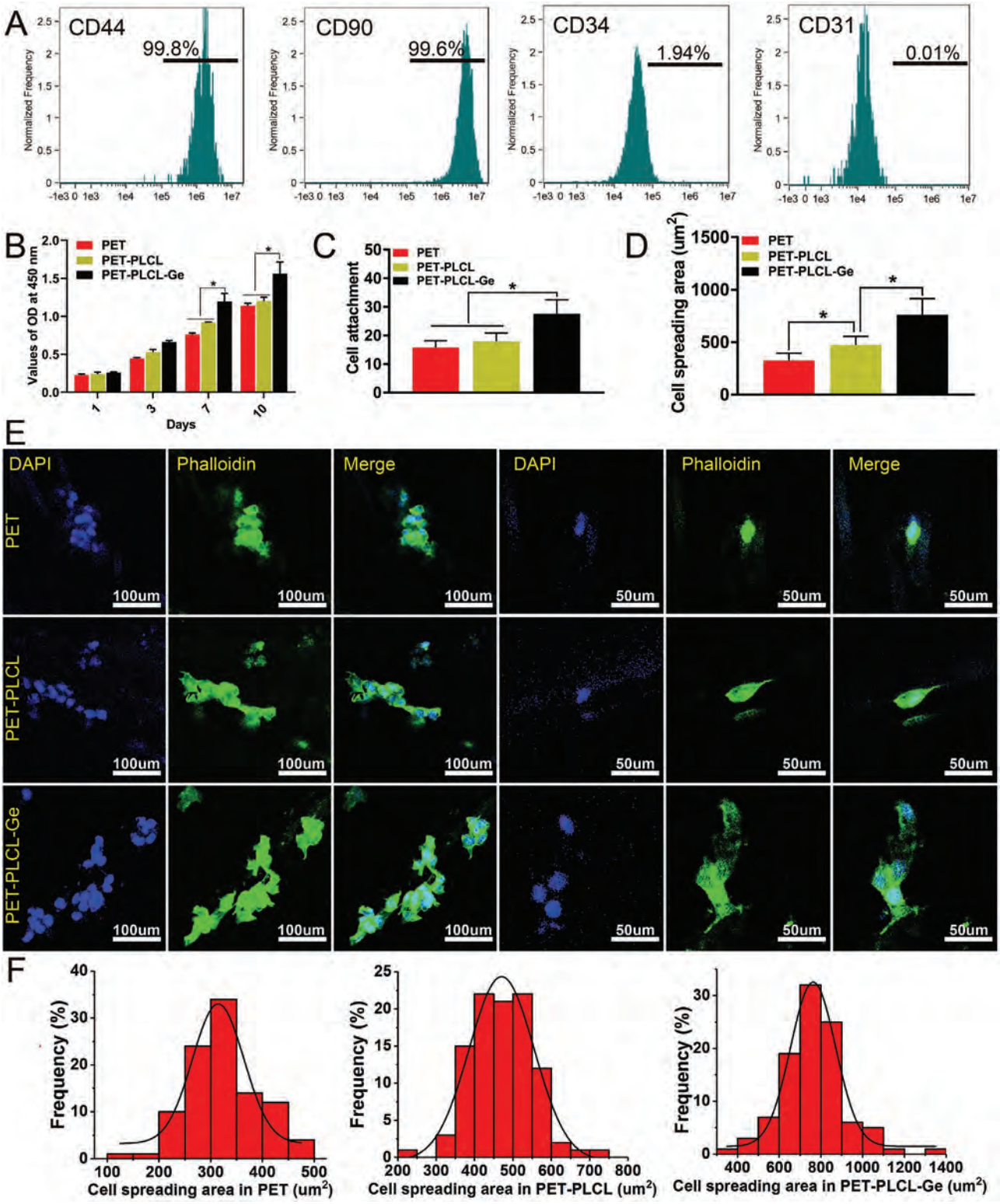

Figure 4. Cytotoxicity measurement of anisotropic hybrid nanofibrous composites in vitro. A) TDSCs were analyzed and confirmed by flow cytometry. The obtained cells were positive for CD44 and CD90, while negative for CD31 and CD34. B) CCK-8 assay results of TDSCs cocultured with PET, PET-PLCL, and PET-PLCL-Ge composites. The data were statistically analyzed by the Student's *t*-test. ($n = 3$; * represented $p < 0.05$.) C) Comparison of cell attachment amount in PET, PET-PLCL, and PET-PLCL-Ge yarns. ($n = 5$; * represented $p < 0.05$.) D) Comparison of cell spreading area in PET, PET-PLCL, and PET-PLCL-Ge yarns. ($n = 100$; * represented $p < 0.05$.) E) DAPI and Phalloidin staining of TDSCs coculturing in PET, PET-PLCL, and PET-PLCL-Ge yarns. (Confocal microscopy: bar = 100 um and 50 um) F) The histogram of cell spreading area distribution for TDSCs attached in PET, PET-PLCL, and PET-PLCL-Ge yarns. ($n = 100$)

 © 2022 Wiley-VCH GmbH

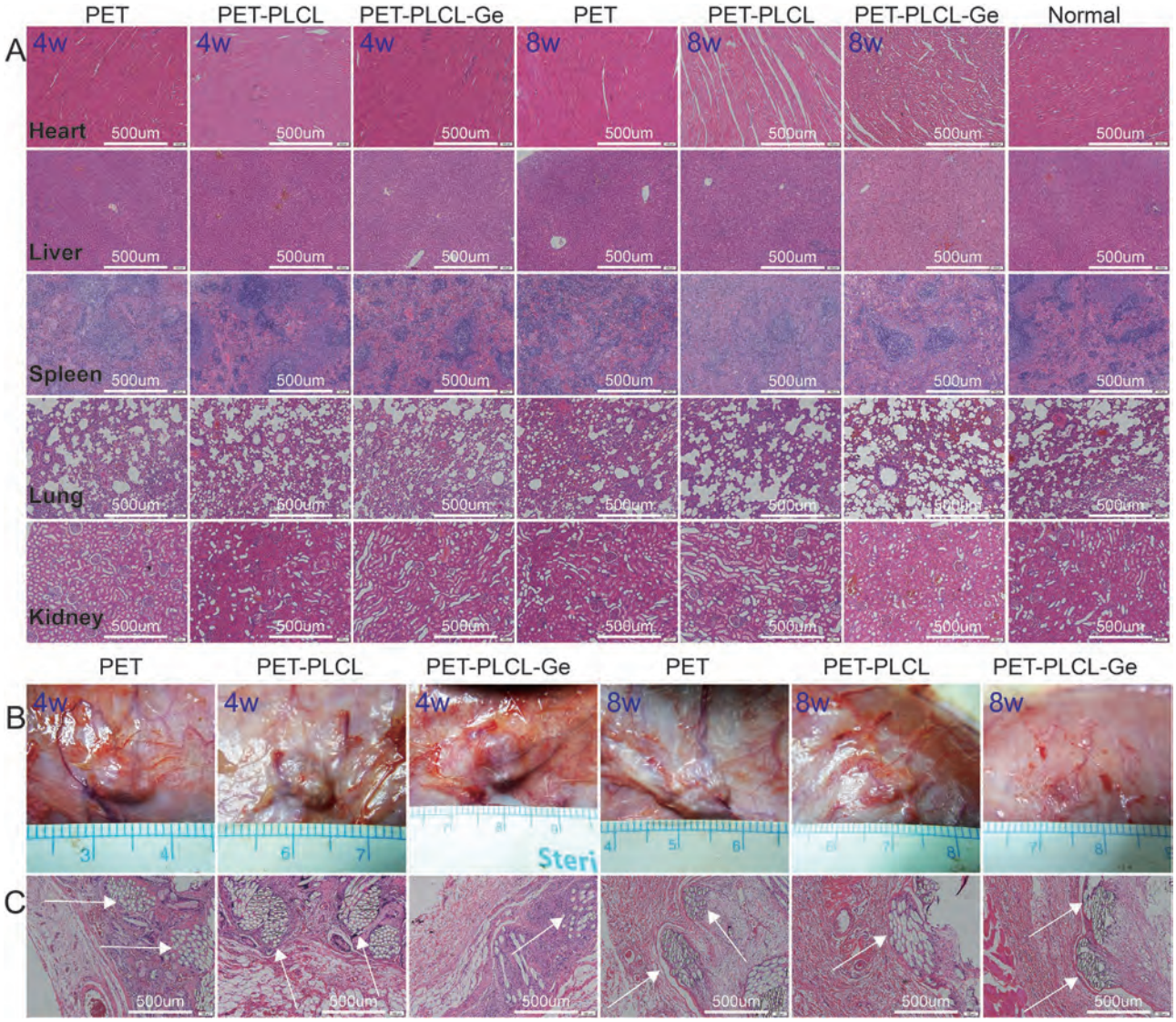

Figure 5. Evaluation of biocompatibility and biodurability for anisotropic hybrid nanofibrous composites after subcutaneous implantation in vivo at different time points. A) The measurement of systemic toxicity in vivo through histologically evaluating visceral organs of heart, liver, spleen, lung, and kidney. (bar = 500 um) B) Macroscopic observation of knitted PET, PET-PLCL, and PET-PLCL-Ge scaffolds at 4 and 8 weeks. C) Local histocompatibility analysis was performed by HE staining. Arrows pointed nondegraded PET fibers. (bar = 500 um)

of fibers, there was also a relative movement of physical abrasion causing the loss of materials in form of particles or wear debris, which acted as the initiator of synovitis to aggravate biocorrosion. Thus, it was essential to optimize corrosion resistance by focusing on and treating the surface rather than by chemically manipulating the raw materials. In this study, PLCL wrapped PET fibers together as an intermediate sheath to prevent fiber-on-fiber relative movement. PLCL was highly hydrophobic that only allowing minimal amounts of body fluids to penetrate into PET fibers. As a result, PET fibers were protected in core and exerted long-term functionality.

In the outer layer, gelatin nanofibrous matrices were electrospun to make the surface hydrophilic and more biocompatible. Gelatin possessed the RGD sequences of collagen to facilitate cell adhesion. After implantation in vivo, gelatin degraded rapidly and surrounding tissues propagated along gelatin nanofibers to penetrate between individual hybrid yarns. As a result, this unique structure effectively reduced the relative movement between two yarns to avoid generating wear particles for synovitis. Moreover, surrounding tissues infiltrated into the nanofibrous composites, several outcomes were obtained. First, the ingrown tissue between hybrid nanofibrous yarns can provide nutrients for tendon/ligament repair and regeneration. Second, the tissue sheaths that surround implanted hybrid nanofibrous yarns are anisotropic and can isolate PET-PLCL from host tissue matrix. Third, tissue sheaths can reduce yarn-on-yarn or yarn-on-bone abrasion and a concomitant decrease in friction-generated wear particles, with accompanying decrease in synovitis and subsequent cartilage damage.

 © 2022 Wiley-VCH GmbH

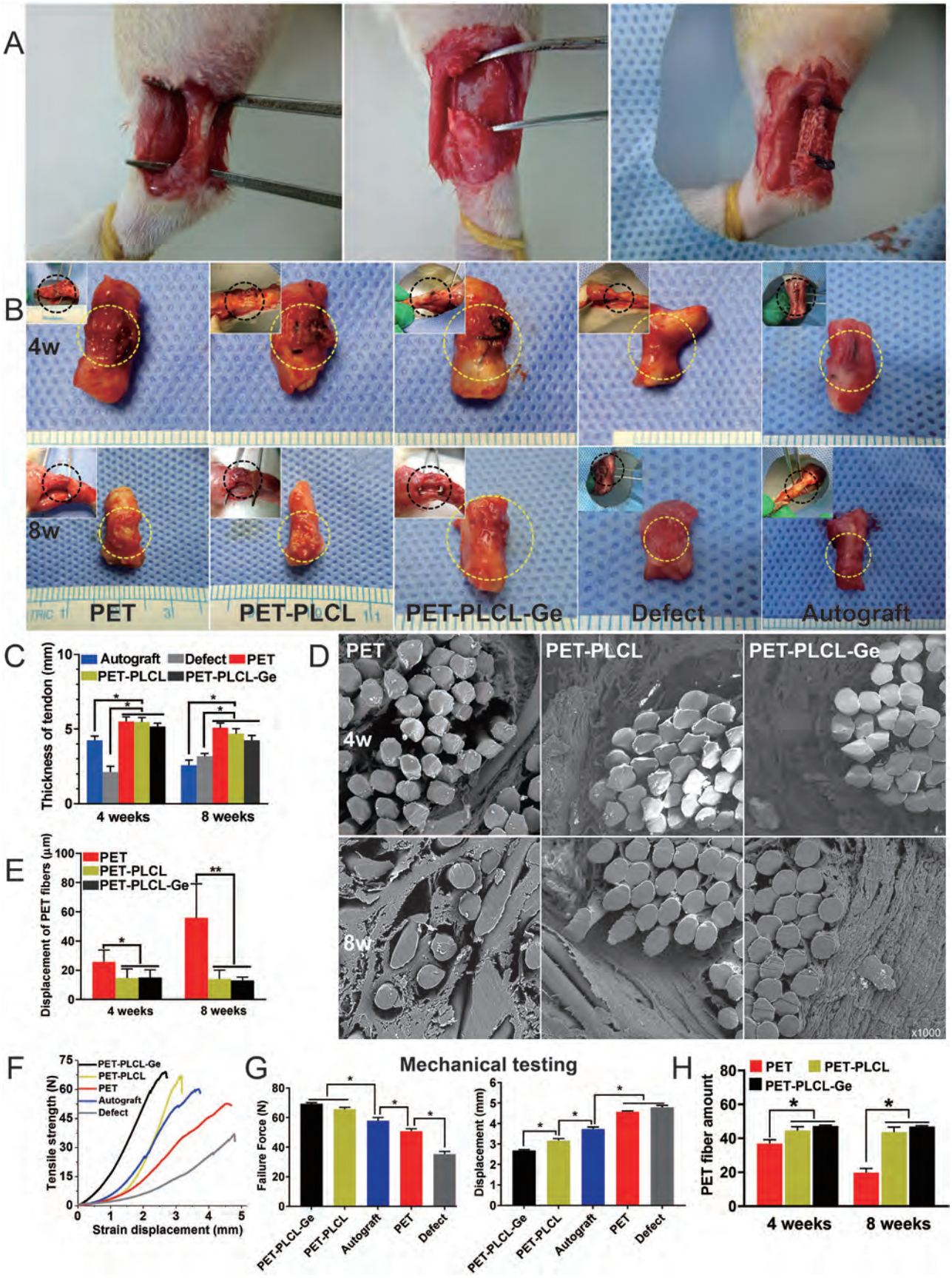

© 2022 Wiley-VCH GmbH

2.6. Tissue Integration Property of Anisotropic Knitted Nanofibrous Composites

Anisotropic hybrid nanofibrous composites were designed with highly porous and interconnected pore structure to serve as a suitable template for guiding surrounding tissue ingrowth in vivo. In this study, a 5 mm Achilles tendon defect was established in rats and repaired with different nanofibrous composites to investigate their efficacy in the treatment of T/L rupture (**Figure 6**A). Before implantation into tendon defects, rat TDSCs were cultured on nanofibrous composites for 7 days to form cell-scaffold constructs in vitro. The rats sutured with autogenous tendons were used as normal repair group. Achilles tendon defects without suture were used as defect group.

At 4 weeks after implantation, the newly formed tendons were retrieved to observe the gross morphology (Figure 6B). Composite ligaments were obviously reddened and surrounded by abundant vasculature. Collagenous tissue infiltration into nanofibrous composites was partly organized and incomplete. The surface was rough and interconnected textile structure was still observed in the formed tendons treated with all types of nanofibrous composites. The tendons repaired with artificial ligaments did not become thinner, while nontreated tendon in the defect group was drastically thinner. With the duration of implantation, the extent of collagenous infiltration increased into the textile structure. At 8 weeks, the gross appearance changed and became smooth in all nanofibrous composite groups. Compared with PET and PET-PLCL groups, the surface of PET-PLCL-Ge group was smoother, indicating that healing inside PET-PLCL-Ge composites was fully organized and complete. Furtherly, we compared the thickness of formed tendons, and found that the thickness in three composite groups was all higher than that in normal repair and defect groups (Figure 6C). This indicated that the knitted structure successfully guided more surrounding tissue growth into nanofibrous composites.

On the other hand, SEM was used to observe the integration of different anisotropic hybrid nanofibrous composites with the host tendon tissue (Figure 6D). At 4 weeks after implantation, the surrounding tissue was noticeably separable from PET and PET-PLCL composites. The detectable gaps were noticed between PET or PET-PLCL composites and host tissue matrix, that most probably due to the hydrophobic property of materials. Even after 8 weeks, there was still a detectable gap between PET composites and host tendon tissue. Moreover, the PET fibers were integrated with the tendon tissue in a scattering appearance, not in gathered bundles. After wrapping with PLCL, PET fibers were bonded more closely in vivo for PET-PLCL and PET-PLCL-Ge groups (Figure 6E). In comparison to PET and PET-PLCL composites, tendon repair with PET-PLCL-Ge composites led to significantly close tissue integration at the tissue-scaffold interface. Surrounding PET-PLCL-Ge yarns there was no crack in the transition zone. The potential mechanism for this phenomenon may be attributed to the outer layer of gelatin nanofibrous matrices. As a biocompatible interfacial element, gelatin significantly enhanced the integration with the host tissue matrix.

Correspondingly, formed tendons in PET-PLCL-Ge group attained the best mechanical strength and histological structure. In the mechanical assessment of formed tendons, we found that PET-PLCL-Ge group exhibited the strongest failure force and lowest strain displacement among all groups (Figure 6F–G). This was related to the material composition and hierarchical structure of PET-PLCL-Ge knitted ligament.

In addition, macroscopic observation of the textile ligaments in tendon showed that the composites underwent limited degradation over 8 weeks. The SEM examination for all three types of nanofibrous composites showed that PET fibers remained complete and ECM deposition was visible surrounding the yarns (Figure 6D). After 8 weeks, the structure of PET yarn was destroyed, while PET-PLCL and PET-PLCL-Ge yarns maintained intact structure. We quantitatively analyzed the alignment of PET fibers in vivo to assess their fatigue properties. At 4 and 8 weeks, the number of filaments in PET composite was significantly lower than PET-PLCL-Ge and PET-PLCL composites (Figure 6H). This was ascribed to yarn abrasion and loose property of PET composite. In the PET-PLCL and PET-PLCL-Ge composites, the number of fibers and alignment did not change significantly, which were equal to their initial conditions ex vivo. Thus, these morphological findings suggest that PET-PLCL-Ge composite can maintain structural integrity in vivo while promoting tendon tissue repair and functioning effectively to substitute tendons or ligaments.

2.7. Capacity of Anisotropic Knitted Nanofibrous Composites for Ligamentization and Remodeling In Vivo

In clinical studies, LARS ligaments have been reported to exhibit an effective clinical outcome for ligament reconstruction, but there is overall complication rate of 5.7% including joint synovitis and artificial ligament rupture.[34] Serious synovitis was reported to have an association with poor ligamentization and remodeling of artificial ligaments after implantation in vivo, which can result in graft rupture and surgical failure.[35]

T/L repair involves the initial proliferation of tendon progenitor cells followed by interstitial deposition of extracellular matrix. After implantation, the nanofibrous composites

Figure 6. A) Surgical procedure of Achilles tendon defect and repair with different nanofibrous composites in SD rats. B) Macroscopic observation of Achilles tendon tissue samples at 4 and 8 weeks after implantation. C) Thickness comparison of the newly regenerated tendons at 4 and 8 weeks postoperatively. ($n = 5$; * represented $p < 0.05$.) D) SEM images of the knitted PET, PET-PLCL, and PET-PLCL-Ge nanofibrous composites at 4 and 8 weeks after implantation. E) The assessment of fiber displacement among PET, PET-PLCL, and PET-PLCL-Ge nanofibrous composites at 4 and 8 weeks after implantation. (The data were expressed as the mean ± SD. $n = 5$; * represented $p < 0.05$.) F,G) Mechanical testing of the regenerated tendons (stress-strain curve, failure force, and failure strain) at 8 weeks after the operation. (The data were expressed as the mean ± SD. $n = 3$; * represented $p < 0.05$.) H) Quantitative assessment of aligned PET fibers in vivo at 4 and 8 weeks after implantation. (The data were expressed as the mean ± SEM. $n = 5$; * represented $p < 0.05$.) PET, PET-PLCL, and PET-PLCL-Ge groups were repaired with PET, PET-PLCL, and PET-PLCL-Ge composites respectively. The defect group was repaired without any treatment. The autograft group was repaired with autogenous tendon. All data were statistically analyzed by the Student's *t*-test.

 © 2022 Wiley-VCH GmbH

underwent ligamentization and remodeling processes to transform into the structure analogous to native T/L. The long-term functionality was directly associated with the quality of graft ligamentization. Poor ligamentization and remodeling in vivo foreboded a great possibility of graft rupture and surgical failure. In order to evaluate the quality of the newly formed tendon, histological analyses were performed including hematoxylin-eosin (HE), Masson's trichrome (MT), and toluidine blue (TB) staining (**Figure 7**A).

At 4 weeks after implantation, HE staining showed that large quantity of host cells migrated into the interior of composites in all scaffold groups. The infiltrated cells were mainly inflammatory cells and proliferative cells (Yellow arrows). The newly formed tendon tissue was characterized by a high ratio of the cell to extracellular matrix. At 8 weeks, plenty of extracellular matrix was deposited and assembled in a regular organized order (Yellow arrows). The nuclear staining confirmed that infiltrated cells showed a significant decrease in all groups over time. This was in accordance with histological changes observed in autograft repair group.

In the PET composite group, HE staining showed loose fiber-by-fiber arrangement in the yarn and complete penetration of surrounding tissue into the internal fibers at 4 weeks (White arrows). The infiltrating tissue was responsible for separating PET yarns into individual fibers. With the time of implantation, the PET yarn was furtherly disintegrated in a messy appearance at 8 weeks (Figure 7A). This was detrimental to the long-term functionality of nanofibrous composites to substitute T/L. Compared with PET composite, PET-PLCL and PET-PLCL-Ge composites exhibited a close and compact fiber-by-fiber arrangement at 4 weeks and even 8 weeks (Figure 7A). This was attributed to the intermediate sheath of PLCL nanofibers, which prevented surrounding tissue from penetrating into PET fibers. In the PET-PLCL composite group, there was an obvious fibrous capsule around hybrid yarn at 8 weeks (Black arrows). This was caused by the acute attack from cells and chemical agents (such as oxidants and enzymes) on the surface of hydrophobic PLCL layer. After improving biocompatibility by gelatin nanofibrous matrices, there was less fibrous capsule around PET-PLCL-Ge yarn at 8 weeks (Black arrows). In the core of PET-PLCL-Ge composite, there were regular infiltration of collagenous tissue between interloping yarns. The penetrated collagenous tissue was in charge of separating hybrid nanofibrous yarns within PET-PLCL-Ge composite, but not PET fibers within the yarn.

Furthermore, MT staining was performed to demonstrate the histomorphological rearrangement of collagenous tissue. There were usually two types of collagen fibers in newly formed tendon tissue, including mature (MT staining red) and immature collagen fibers (MT staining blue). At 4 weeks there were almost immature collagen fibers in all scaffold groups and no difference was observed between groups (Red arrows). After 8 weeks, mature collagen fibers were observed and abundant in PET-PLCL-Ge composite while rare in PET and PET-PLCL composites. Moreover, mature collagen fibers in PET-PLCL-Ge composite were highly aligned and comparable to autograft repair group, indicating that the PET-PLCL-Ge composite provided a comparable remodeling performance to normal tendon repair. In the analysis of TB staining, the regenerated tendon tissue in PET-PLCL-Ge composite achieved the histomorphological quality comparable to autograft repair after 8 weeks, which was significantly better than PET or PET-PLCL composites. In the evaluation of histological score, PET-PLCL-Ge group was significantly higher than PET and PET-PLCL group, while equal to autograft repair group (Figure 7B).

2.8. Tendon Regeneration and Related Extracellular Matrix Deposition of Anisotropic Knitted Nanofibrous Composites

The crucial hallmark of successful tendon ligamentization is the extensive deposition of tendon-related extracellular matrix and proteins in the regenerated tendons. In this study, immunohistochemical staining and semiquantitative analyses were performed to assess the synthesis of various tendon-associated extracellular matrix proteins (Figure 7C,D).

The most abundant form of collagen in tendon is type I collagen fibrils which is a stiff structure to provide the tendon with its mechanical strength and biodurability.[36] Collagen III is another collagen fibril that has always been involved in the regeneration process of tendon. At 8 weeks after implantation, the immunohistochemical staining of Collagen I and Collagen III in PET-PLCL-Ge composite was obviously stronger than that in PET and PET-PLCL composites (Blue arrows). Therefore, we inferred that the higher mechanical strength of formed tendon in PET-PLCL-Ge composite than PET and PET-PLCL composites was also due to the more abundance of regenerated Collagen I and Collagen III.

Decorin (DCN), as a small leucine-rich proteoglycan, plays an essential role in collagen fibril and matrix assembly. It is necessary to maintain collagen fibril structure, fiber realignment, and mechanical properties of mature tendon.[37] In this study, the immunohistochemical staining of DCN in PET-PLCL-Ge composite was also stronger than that in PET and PET-PLCL composites (Blue arrows). Thus, DCN was associated with collagen I and collagen III together to complete the maturation of the extracellular matrix in tendon.

Tenascin C (TNC), another important protein of tendon ECM, is typically used as a molecular marker for tendon regeneration.[38,39] It was expressed at the site of the injured tendon to aid cell migration and dynamic arrangement of ECM during tissue ligamentization and remodeling.[40,41] As shown in Figure 7C, the staining intensity of TNC in PET-PLCL-Ge group was higher than that in PET and PET-PLCL groups. Consequently, the more regular arrangement of the extracellular matrix was achieved in PET-PLCL-Ge group, which was shown in Figure 7A (Red arrow at 8w Masson).

Then semi-quantification of immunohistochemical staining was performed to further analyze the statistical differences between different groups. Among the three scaffold groups, collagen I, collagen III, and DCN of PET-PLCL-Ge group was the most obvious. Moreover, the density of collagen I, collagen III, and DCN in PET-PLCL-Ge group was significantly higher than that in autograft group (Figure 7D). This was mainly due to the engraftment of TDSCs in PET-PLCL-Ge group, while no TDSCs in autograft group. The immunofluorescent staining also confirmed the stronger staining intensity of collagen I and collagen III in PET-PLCL-Ge group than PET and PET-PLCL groups (Supporting Information Figure S10, Supporting Information).

 © 2022 Wiley-VCH GmbH

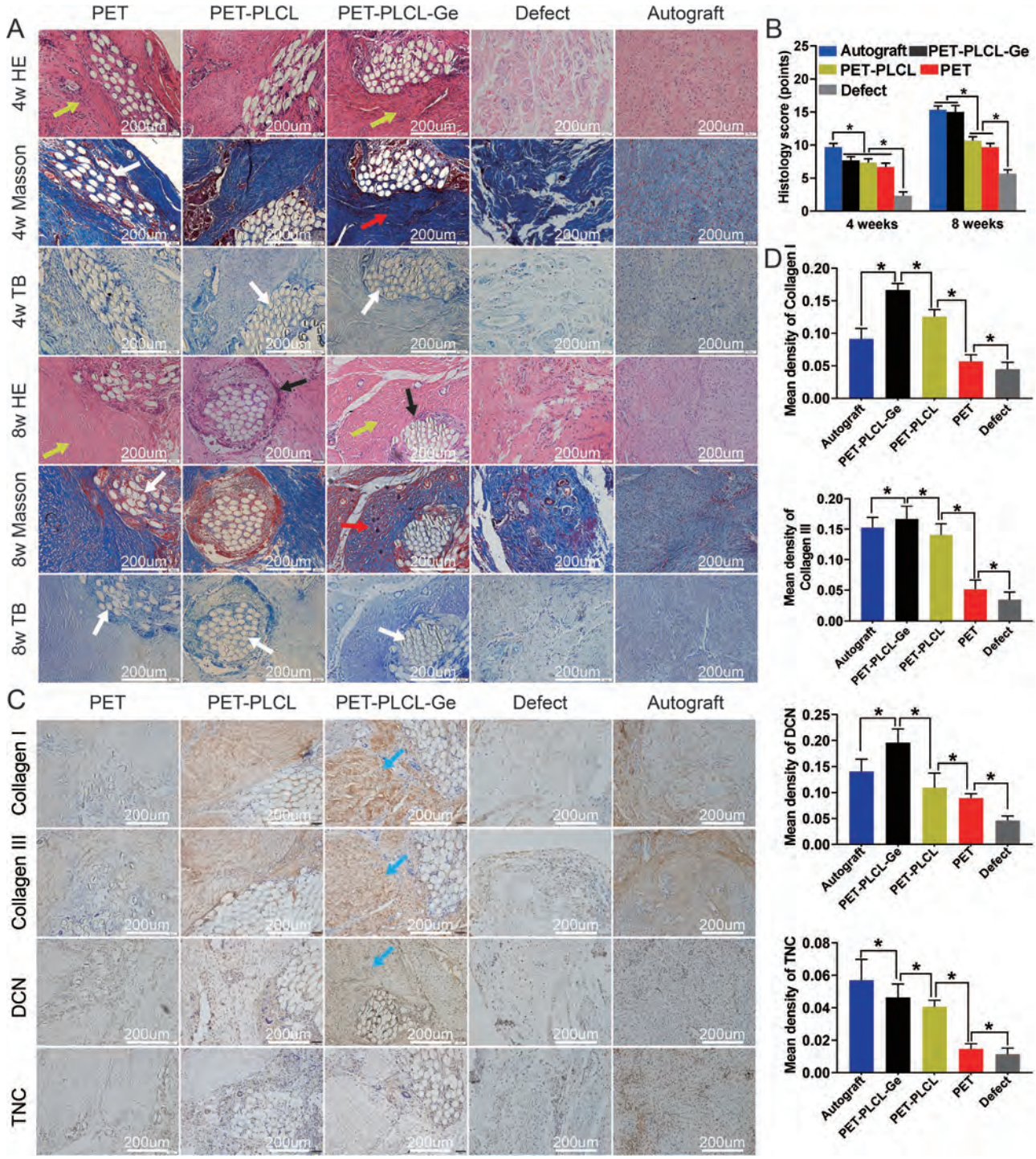

Figure 7. A) Histological staining of formed tendons was analyzed at 4 and 8 weeks postoperatively, including hematoxylin-eosin (HE), Masson's trichrome (MT), and toluidine blue (TB). Yellow arrows indicated mainly proliferative cells at 4 weeks and plenty of extracellular matrix at 8 weeks. White arrows showed PET fibers. Black arrows indicated fibrous capsule around PET-PLCL yarn while no around PET-PLCL-Ge yarn. Red arrows indicated immature collagen fibers at 4 weeks and mature collagen fibers at 8 weeks. B) Histological score was evaluated according to histological staining at 4 and 8 weeks postoperatively. The data were statistically analyzed by the Student's *t*-test and expressed as the mean ± SD. $n = 5$; * represented $p < 0.05$. C) Immunohistochemical staining of formed tendons was analyzed at 8 weeks postoperatively for collagen I, collagen III, DCN, and TNC. Blue arrows indicated the immunohistochemical staining of collagen I, collagen III, and DCN. D) The semi-quantitative analysis was performed according to immunohistochemical staining at 8 weeks postoperatively. The data were statistically analyzed by the Student's *t*-test and expressed as the mean ± SD. $n = 5$; * represented $p < 0.05$.

 © 2022 Wiley-VCH GmbH

These results indicated that PET-PLCL-Ge knitted composite could promote in vivo tenogenic differentiation and maturation of formed tendon, which was likely to be triggered by the outer layer of gelatin nanofibrous matrices in hybrid yarns.

3. Conclusion

In this study, a novel strategy was proposed to fabricate hybrid nanofibrous composites with anisotropic mechanical properties and hierarchical structure as superior artificial ligaments. Three-layered nanofibrous yarns were produced to improve biocompatibility and biodurability of PET fibers. Then hybrid yarns were customized with knitted structure, providing porous and interconnected pores to reduce fiber-to-fiber abrasion, which was the main cause for severe synovitis and high failure rate of LARS ligament in clinical application. Especially in mechanical behavior, the knitted nanofibrous composites exhibited stronger and tougher mechanical properties than native T/L, as well as the equivalent anisotropic characteristics. Furthermore, after replacing native tendon, PET-PLCL-Ge knitted composite was successfully integrated with native tissue, in which normal functionality of T/L was attained not only at the mechanical level but also at the level of related extracellular matrix deposition. Overall, this study provides a new method for designing knitted nanofibrous composites with anisotropic properties to develop new artificial ligaments for clinical T/L replacement.

4. Experimental Section

Materials: Unless otherwise mentioned, all reagents in this experiment were purchased from Sigma-Aldrich. The cell markers (CD90, CD31, CD34, CD44) and α-SMA antibody were purchased from Thermo Fisher. The cell multi-differentiation induction kits were purchased from Cyagen Biosciences Inc, China.

Synthesis of PET-PLCL: We employed PET yarns (90% crystalline, line density 240D) containing 48 filaments (line density 5D) in a yarn to synthesize PET-PLCL hybrid nanofibrous yarns. A single PET yarn was pulled through a rotating funnel as the core layer. And 1.0 g PLCL was dissolved in 10 mL hexafluoroisopropanol to produce PLCL solution at the concentration of 10%. The funnel was rotated to add PLCL nanofibers onto the surface of PET yarn. The receiving roller was used to collect PET-PLCL double-layer nanofiber yarn.

The specific process of electrospinning is as follows: the spinning solution was added into two syringes, which were connected to the spinning nozzles on both sides of the yarn respectively. With the application of 8KV for positive and negative electrodes, PLCL solution was dispensed at a rate of 1.2 mL h^{-1}, locating a distance of 12 cm to the rotating funnel. The funnel was rotated at the speed of 400 rpm, and the receiving roller's speed was 8 rpm. The following yarns were also prepared according to this process.

Synthesis of PET-PLCL-Ge: 1.2 g gelatin (Ge) was dissolved in 10 mL trifluoroethanol to produce Ge solution at the concentration of 12%. The PET-PLCL nanofiber yarn was pulled through the rotating funnel as the core layer. Ge solution was sprayed and added to the surface of PET-PLCL by rotating funnel to yield PET-PLCL-Ge three-layer nanofiber yarn. The weight ratio of PET, PLCL, and Gelatin was 10:1:2 in the composite yarn. Then, Ge nanofibers were chemically cross-linked with glutaraldehyde steam, and subsequently soaked into L-glutamate solution to remove the residual glutaraldehyde.

Scaffold Manufacturing Technology: Three textile configurations were manufactured including nonwoven, woven, and knitted fabrics and then compared with LARS ligament that was used in clinic. Nonwovens were produced from nanofibers through the electrospinning technique.[42,43] Woven fabrics were produced by weaving weft yarns above and below warp yarns to form a plain weave structure.[44] Knitted fabrics were produced by a computerized knitting machine based on previous literature to get interlocked geometry.[45]

Morphology Characterization: I) The composites were gold-coated and observed using scanning electron microscope (SEM) to compare the surface appearance of different scaffolds. II) Water contact angle assessment: the electrospinning fabrics were cut into approximately 1 × 1 cm (n = 6) pieces. One droplet of distilled water was gently deposited on each sample through a micro syringe. The images were captured, and water contact angle was measured by the inbuilt software of a commercial drop shape analysis system (Data Physics SCA20, Germany). III) X-ray diffraction (XRD): the sample was cut into about 3 cm × 1 cm, and placed on the XRD instrument's (D/max-2550, Japan) loading pad. The diffraction intensity curve of $2\theta = 10 - 80°$ was recorded at the scanning speed of 5° min^{-1} with CuKα rays of λ = 1.54 nm, pipe voltage of 40 kV, and pipe current of 35 mA. IV) Fourier transform infrared spectroscopy (FTIR, NEXUS-670, USA). The scanning range was 400–4000 cm^{-1}, and the resolution was 4 cm^{-1}. V) Mechanical test: the scaffold or the yarn was fixed to the mechanical testing machine (H5K-S, Hounsfield, UK) with a distance of 20 mm. The tensile test was carried out at a pull speed of 5 mm min^{-1} until the scaffold or the yarn broke. Then stress-strain curves were constructed from the load-deformation curves. The strength, elastic modulus, and breaking elongation were calculated from plotted stress-strain curves.

Cell Isolation and Identification: All animal experiments were approved by the Ethics Committee on Animal Experiments of Shanghai Tenth People's Hospital (No. SHDSYY-2018-4427). Cell isolation was performed according to the previous studies.[46,48] In brief, 4-week-old male Sprague Dawley (SD) rats (SLAC laboratory animal CO.LTD, Shanghai, China) were executed with 10% hydrated chloral overdose anesthesia. Achilles tendons were harvested from the rat hindlimb and minced into small pieces. Achilles tendons were digested with 3 mg mL^{-1} type I collagen enzymes for 2 h at 37 °C, and then filtered to obtain tendon-derived stem cells (TDSCs). The cells were collected and cultured in low-glucose Dulbecco's Modified Eagle's Medium (DMEM) supplemented with 10% fetal bovine serum (FBS) at 37 °C and 5% CO_2.

Antibodies (including anti-Collagen I, CD90, CD31, CD34, CD44, α-SMA) were applied to identify TDSCs with immunofluorescence and flow cytometry technology (BD FACSLyric, USA). Then, the multi-lineage differentiation potential of TDSCs was performed with Cyagen kits (RASMX-90021, RASMX-90031, RASMX-90041, Cyagen Biosciences, Guangzhou, China) according to the manufacturer's instructions.

Biocompatibility and Biotoxicity of the Scaffolds: The scaffolds were fumigated overnight with alcohol and irradiated with ultraviolet rays for 30 min. The scaffolds were washed with PBS 3 times and placed in a 24-well tissue culture plate with culture medium overnight. After that, TDSCs were seeded in the plate at the dense of 1×10^6 cells per mL. Cells were cultured with different scaffolds for 1, 3, 7, and 10 days. Cell Counting Kit-8 (CCK-8) was used and the absorption was evaluated at 450 nm using a spectrophotometer (Bio-Rad model 550, USA).

Next, TDSCs suspension in a complete medium was prepared at the density of 5×10^4 cells per mL to seed on each scaffold. After 3 days the cells were stained by DAPI (4′,6-diamidino-2-phenylindole, Solarbio, Beijing, China) and FITC-conjugated phalloidin (MedChem Express). All groups were observed using confocal and fluorescence microscopes. The number of cells attached on the surface of scaffolds was counted in five randomly-selected fields. The cell spreading areas were estimated using image analysis software (Image-J, National Institutes of Health, USA) to calculate 100 cells randomly observed on the fluorescent images.

Then, the scaffolds were cut into 10 mm by 10 mm and buried under the skin of SD rats respectively. After 4 and 8 weeks, scaffolds as well as

 © 2022 Wiley-VCH GmbH

the hearts, livers, spleens, lungs and kidneys were obtained to assess the toxicity and biocompatibility by HE staining.

Rat Achilles Tendon Injury Model: In vivo study was performed using eight-week-old SD rats with eight rats in each group. The procedures were performed according to the previous reports.[49,50] All animal experiments were approved by the Ethics Committee on Animal Experiments of Shanghai Tenth People's Hospital (No. SHDSYY-2018-4427). After anesthesia with 10% chloral hydrate, achilles tendon was excised 5 mm distance from the terminal point and a 5-mm defect was created in the right hindlimb. The defect was repaired with the composites or autografts by suturing on both sides. The defect was repaired without any scaffold to serve as control group (defect group). Rats were randomized into defect group, autograft group, PET+TDSCs group, PET-PLCL+TDSCs group, and PET-PLCL-Ge+TDSCs group. After surgery, SD rats were individually housed in isolated cages to restrict their movements.

Histological Evaluation: I) At 4 and 8 weeks after operation, the rats were sacrificed by overdose anesthesia to obtain achilles tendons. II) Mechanical test. The obtained achilles tendon were tested on the mechanical testing machine (H5K-S, Hounsfield, UK), and analyzed with the inbuilt testing system. III) SEM examination. The achilles tendon tissues of different groups were fixed in 4% paraformaldehyde solution, washed 3 times with PBS, dehydrated with gradient alcohol (50–100%), lyophilized, and plated with gold (2 min, 20 mA). SEM (Phenom XL, Netherlands) was used to observe the healing condition. IV) Histological analysis: Briefly, after being fixed in 4% paraformaldehyde solution, tissues were dehydrated, embedded in paraffin, and cut into 5 µm thick slices. The sections were then stained with hematoxylin-eosin (HE), Masson's trichrome, and toluidine blue. Immunohistochemical assays were also performed including collagen I, collagen III, TNC, and DCN.

Statistical Analysis: All experiments were performed on three replicates, unless otherwise mentioned. All quantitative data were statistically analyzed by using IBM SPSS Statistics 19.0 and GraphPad Prism 8.0 software. The data were presented as the mean ± standard deviation (SD). The statistically significant difference was indicated with asterisks and p-values via the Student's *t*-test. (* represented $p < 0.05$.)

Supporting Information

Supporting Information is available from the Wiley Online Library or from the author.

Acknowledgements

J.L., C.X., and H.W. contributed equally to this work. This study was supported by the National Nature Science Foundation of China (81802144, 81702133), the Research Project of Shanghai Municipal Health Commission (Contract Grant No. 20194Y0316), and the Excellent Youth Training Program of Shanghai Jiaotong University Affiliated Sixth People's Hospital (ynyq202102).

Conflict of Interest

The authors declare no conflict of interest.

Data Availability Statement

The data that support the findings of this study are available from the corresponding author upon reasonable request.

Keywords

anisotropic architecture, biocompatibility, mechanical durability, nanofibrous composites, tendon/ligament repair

Received: February 21, 2022
Revised: May 12, 2022
Published online:

[1] S. Claes, E. Vereecke, M. Maes, J. Victor, P. Verdonk, J. Bellemans, *J. Anat.* **2013**, *223*, 321.
[2] M. J. Kraeutler, K. L. Welton, J. Chahla, R. F. LaPrade, E. C. McCarty, *Am. J. Sports Med.* **2018**, *46*, 1235.
[3] L. David, E. S. Grood, F. R. Noyes, R. E. Zernicke, *Exercise Sport Sci. Rev.* **1978**, *6*, 125.
[4] C. B. Frank, D. A. Hart, N. G. Shrive, *Osteoarthritis Cartilage* **1999**, *7*, 130.
[5] K. F. Bowman Jr, J. K. Sekiya, *Sports Med. Arthrosc. Rev.* **2010**, *18*, 222.
[6] V. Guarino, A. Guaccio, L. Ambrosio, *J. Appl. Biomater. Biomech.* **2011**, *9*, 34.
[7] M. Laranjeira, R. M. Domingues, R. Costa-Almeida, R. L. Reis, M. E. Gomes, *Small* **2017**, *13*, 1700689.
[8] P. Wei, T. Chen, G. Chen, K. Hou, M. Zhu, *ACS Appl. Mater. Interfaces* **2021**, *13*, 19291.
[9] C. Legnani, A. Ventura, C. Terzaghi, E. Borgo, W. Albisetti, *Int. Orthop.* **2010**, *34*, 465.
[10] R. I. Umasabor, S. C. Daniel, *Heliyon* **2020**, *6*, e04700.
[11] H. Li, S. Chen, *J. Biomed. Mater. Res., Part A* **2015**, *103*, 839.
[12] L. Dissanayake, L. N. Jayakody, *Front. Bioeng. Biotechnol.* **2021**, *9*, 656465.
[13] C. Smith, A. Ajuied, F. Wong, M. Norris, D. Back, A. Davies, *Arthrosc.: J. Arthrosc. Relat. Surg.* **2014**, *30*, 111.
[14] J. S. Mulford, D. Chen, *ANZ J. Surg.* **2011**, *81*, 785.
[15] T. M. Tiefenboeck, E. Thurmaier, M. M. Tiefenboeck, R. C. Ostermann, J. Joestl, M. Winnisch, M. Schurz, S. Hajdu, M. Hofbauer, *Knee* **2015**, *22*, 565.
[16] E. J. Olson, J. D. Kang, F. H. Fu, H. I. Georgescu, G. C. Mason, C. H. Evans, *Am. J. Sports Med.* **1988**, *16*, 558.
[17] M.-F. Guidoin, Y. Marois, J. Bejui, N. Poddevin, M. W. King, R. Guidoin, *Biomaterials* **2000**, *21*, 2461.
[18] C. Singh, C. S. Wong, X. Wang, *J. Funct. Biomater.* **2015**, *6*, 500.
[19] S. K. Bhullar, B. K. Özsel, R. Yadav, G. Kaur, M. Chintamaneni, H. S. Buttar, *J. Complementary Integr. Med.* **2015**, *12*, 289.
[20] T. J. Yu, C. Chu, *J. Biomed. Mater. Res.* **1993**, *27*, 1329.
[21] G. Ciapini, G. Nulvesu, E. Ipponi, F. Chiellini, M. Mecacci, E. Giannini, P. Parchi, M. Scaglione, *Surg. Technol. Int.* **2021**, *39*, 369.
[22] Y. Cai, D. M. Mitrano, R. Hufenus, B. Nowack, *Environ. Sci. Technol.* **2021**, *55*, 8001.
[23] M. Kuzmanović, L. Delva, L. Cardon, K. Ragaert, *Adv. Mater.* **2020**, *32*, 2003938.
[24] R. Kheirjou, J. S. Rad, A. F. Khosroshahi, L. Roshangar, *Cell Tissue Banking* **2021**, *22*, 225.
[25] E. A. Makris, A. H. Gomoll, K. N. Malizos, J. C. Hu, K. A. Athanasiou, *Nat. Rev. Rheumatol.* **2015**, *11*, 21.
[26] E. Mariani, G. Lisignoli, R. M. Borzì, L. Pulsatelli, *Int. J. Mol. Sci.* **2019**, *20*, 636.
[27] T. Furuike, T. Chaochai, T. Okubo, T. Mori, H. Tamura, *Int. J. Biol. Macromol.* **2016**, *93*, 1530.
[28] C. Wang, W. Huang, Y. Zhou, L. He, Z. He, Z. Chen, X. He, S. Tian, J. Liao, B. Lu, *Bioact. Mater.* **2020**, *5*, 82.

© 2022 Wiley-VCH GmbH

[29] D. Y. Fozdar, P. Soman, J. W. Lee, L. H. Han, S. Chen, *Adv. Funct. Mater.* **2011**, *21*, 2712.
[30] Y. J. No, M. Castilho, Y. Ramaswamy, H. Zreiqat, *Adv. Mater.* **2020**, *32*, 1904511.
[31] C. M. Glezos, A. Waller, H. E. Bourke, L. J. Salmon, L. A. Pinczewski, *Am. J. Sports Med.* **2012**, *40*, 1167.
[32] H. Feng, W. Xing, Y. Han, J. Sun, M. Kong, B. Gao, Y. Yang, Z. Yin, X. Chen, Y. Zhao, *J. Clin. Invest.* **2020**, *130*, 6354.
[33] P. P. Y. Lui, K. M. Chan, *Stem Cell Rev. Rep.* **2011**, *7*, 883.
[34] K. Gao, S. Chen, L. Wang, W. Zhang, Y. Kang, Q. Dong, H. Zhou, L. Li, *Arthrosc.: J. Arthrosc. Relat. Surg.* **2010**, *26*, 515.
[35] H. Li, Z. Yao, J. Jiang, Y. Hua, J. Chen, Y. Li, K. Gao, S. Chen, *Arthrosc.: J. Arthrosc. Relat. Surg.* **2012**, *28*, 583.
[36] M. R. Buckley, E. B. Evans, P. E. Matuszewski, Y. L. Chen, L. N. Satchel, D. M. Elliott, L. J. Soslowsky, G. R. Dodge, *Connect. Tissue Res.* **2013**, *54*, 374.
[37] K. A. Robinson, M. Sun, C. E. Barnum, S. N. Weiss, J. Huegel, S. S. Shetye, L. D. Lin, D. Saez, S. M. Adams, R. V. Iozzo, L. J. Soslowsky, D. E. Birk, *Matrix Biol.* **2017**, *64*, 81.
[38] P. L. Jones, F. S. Jones, *Matrix Biol.* **2000**, *19*, 581.
[39] G. G. Mokone, M. Gajjar, A. V. September, M. P. Schwellnus, J. Greenberg, T. D. Noakes, M. Collins, *Am. J. Sports Med.* **2005**, *33*, 1016.
[40] R. Kluger, K. R. Huber, P. G. Seely, C. E. Berger, F. Frommlet, *Am. J. Sports Med.* **2017**, *45*, 2955.
[41] G. P. Riley, R. L. Harrall, T. E. Cawston, B. L. Hazleman, E. J. Mackie, *Am. J. Pathol.* **1996**, *149*, 933.
[42] N. Bhardwaj, S. C. Kundu, *Biotechnol. Adv.* **2010**, *28*, 325.
[43] H. Yoshida, K. Yanagisawa, *Polymers* **2018**, *10*, 1212.
[44] T. Hua, L. Y. Tang, W. Y. Chiu, X. Tian, *Polymers* **2018**, *10*, 146.
[45] R. Ma, J. Lee, D. Choi, H. Moon, S. Baik, *Nano Lett.* **2014**, *14*, 1944.
[46] T. Harvey, S. Flamenco, C.-M. Fan, *Nat. Cell Biol.* **2019**, *21*, 1490.
[47] Y. F. Wu, C. Chen, J. B. Tang, W. F. Mao, *Stem Cells Dev.* **2020**, *29*, 1016.
[48] P. P. Y. Lui, *J. Cell. Mol. Med.* **2013**, *17*, 55.
[49] J. Huegel, J. F. Boorman-Padgett, C. A. Nuss, M. C. C. Minnig, P. Y. Chan, A. F. Kuntz, E. I. Waldorff, N. Zhang, J. T. Ryaby, L. J. Soslowsky, *J. Biomech.* **2019**, *88*, 194.
[50] M. A. Fernandez-Yague, A. Trotier, S. Demir, S. A. Abbah, A. Larrañaga, A. Thirumaran, A. Stapleton, S. A. Tofail, M. Palma, M. Kilcoyne, *Adv. Mater.* **2021**, *33*, 2008788.

© 2022 Wiley-VCH GmbH